Supporting Information

Plasma-electrolysis synthesis of TiO_2 nano/microspheres with optical absorption extended into infra-red region

By *Zhi-Kun Zhang, Mei-Lin Bai, Deng-Zhu Guo*, Shi-Min Hou*, Geng-Min Zhang*

* To whom correspondence should be addressed: Email: guodz@pku.edu.cn, smhou@pku.edu.cn

1. Experimental and Computational details

1.1 Preparation

The preparation of the TiO_2 nano/microspheres was performed in a simple asymmetric-electrode apparatus, in which a Ti wire and a Pt sheet are immerged in a 3 M NH_4NO_3 solution, serving as the cathode and counter electrode, respectively. The Pt anode has a much larger surface area than that of the cathode, in order to build a sufficiently strong electric field at the Ti cathode. The whole cell was driven with a home-made DC power supply. The voltage was increased from open circuit potential (OCP) at a rate of 1 V/s. The plasma was mostly ignited at 25 V under threshold conditions, i.e., sufficient-high field strength within the gas/vapor sheath and temperature of the solution, accompanied by an abrupt jump of the potential to about 80 V. The cell voltage was then adjusted to 100 V for the stable discharge. After the electrolysis, the precipitation at the bottom was purified with repeated centrifugation and ultrasonic dispersion in deionized water, and finally dried in air.

1.2 Characterization

A scanning electron microscope (SEM, FEI Quanta 600F FEG environmental) and a transmission electron microscope (TEM, Tecnai G20) were employed to characterize the morphologies and structures of the spheres. Energy dispersive X-ray spectroscopy (EDX, accessory in SEM) and X-ray photoelectron spectroscopy (XPS, AXIS Ultra instrument) were used for composition analysis. X-ray diffraction (XRD, Rigaku Dmax/2400) was performed using Cu $K\alpha_1$ (λ=0.15406 nm) at a scanning rate of 4 ° min^{-1}. The current of the cell was monitored with a Keithley 2400, and the emission spectrum of the glow was detected using a fiber optic spectrometer (HR4000, Ocean Optics Co. Ltd. USA).

1.3 Optical measurement

For the optical measurement, TiO_2 spheres and P25 films with nearly identical thickness were prepared on a $BaSO_4$ powder substrate, respectively. The absorption spectra of the samples were then measured by using a Shimadzu UV-3100 spectrophotometer, with a scanning wavelength range from 240 nm to 2600 nm. To confirm the results, the optical measurement was repeated many times.

1.4 Calculation method

The DFT+U scheme is becoming increasingly popular in the study on the electronic properties of semiconducting materials, due to its more accurate results than those of the standard DFT functionals within the local density approximation (LDA) and the generalized gradient approximation (GGA). The Hubbard-U term is added to take into account the strongly correlated nature of Ti *d*-electrons in TiO_2. Our DFT+U calculations were performed by using the Vienna ab initio Simulation Package (VASP) and the GGA exchange-correlation functional within the Perdew-Burke-Ernzerhof (PBE) form was adopted to account for the electron-electron interactions.

The Monkhorst-Pack *k*-point sampling is set as 9×9×9 and the energy cutoff was chosen as 400eV. The spin-polarization was included in all cases. For conciseness, the presence of oxygen vacancies in TiO_2 was modeled by removing one oxygen atom from anatase supercells with 48, 24 and 12 atoms, forming TiO_{2-x} compounds with corresponding x value of 0.063, 0.125 and 0.25, respectively. The TiO_2 supercells in the anatase phase were constructed from the PBE optimized lattice constants a=3.765 Å and c=9.264 Å. Then the atomic positions of all structures were fully optimized. After obtaining the optimized geometry, the densities of states (DOS) of the oxygen-deficient TiO_2 and the corresponding transition rates between those occupied and unoccupied states caused by the interaction with the photons were determined. Finally, the absorption curves were easily obtained from the imaginary part of the dielectric constant, which can be described as a joint density of states between the valence and conduction bands weighted by an appropriate matrix element.

2. Additional results and discussion

2.1 Cathodic plasma electrolysis

Fig. S1a shows a representative current-time (I-t) curve of the electrolysis. There are three main regions during the whole process. Region I is the conventional electrolysis region, in which the current increases with the cell voltage according to the Ohm's law. Region II is the transition region. Since the two electrodes are asymmetric, the electric field is mainly concentrated at the small-size Ti cathode. Therefore, the released heat rapidly raises the temperature of the ambient solution, and generates plenty of vapor bubbles. The vapor bubbles then mix with the gas bubbles from the electrolysis, forming a gas/vapor sheath around the cathode. The growing sheath gradually separates the cathode from the solution and leads to the decrease of the current. The voltage drop thereafter primarily occurs within this sheath, ionizing the internal atom species and causing the plasma. Region III is the plasma region. One can see that the current is primarily kept at a low value after an initial decrease in this region. The oscillation of the current is attributed to the inhomogeneous burst of plasma around the cathode.[1] The key conditions for generating the plasma are found to be the formation of the gas/vapor sheath, the solution temperature, and the cell voltage.

Fig. S1b shows the emission spectrum of the plasma. Comparing with the standard spectral lines,[2] abundant Ti characteristic lines are found (blue squares). This indicates that the Ti atoms are ablated from the cathode by the drastic plasma. Meanwhile, a high peak (red triangle) corresponding to the hydrogen atoms at λ=656.2 nm is detected. The strong reducible H atoms are inferred to be generated by the water electrolysis. The oxygen atoms at λ=777.5 nm (orange circle) are the production of the water splitting in the plasma. Characteristic line for the N species of the solution is absent, probably due to the overlap of the peaks. The left and right insets of Fig. S1b show the digital images of the light-blue-color plasma glow and the black-color precipitation, respectively.

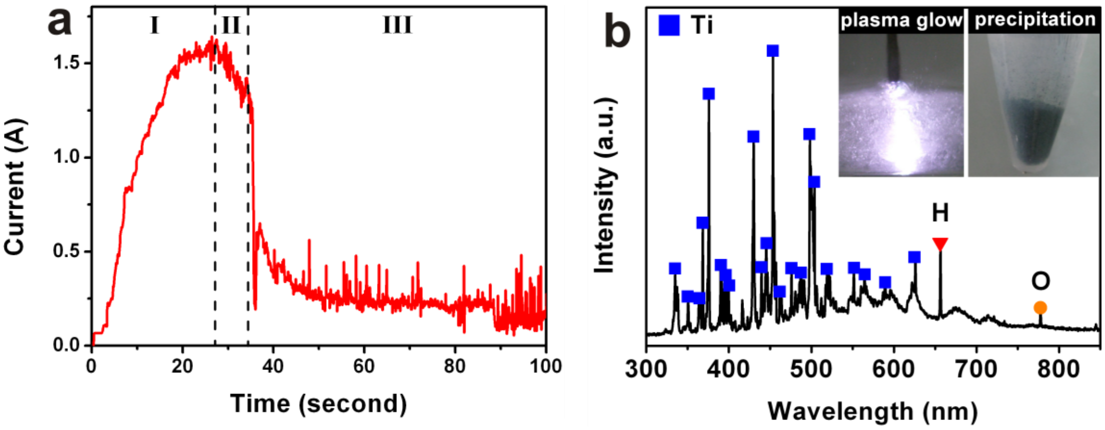

Fig.S1 a) Typical I-t curve of the whole electrolysis process. b) Emission spectrum of the plasma. The insets are digital images of the plasma and as-formed precipitation, respectively.

2.2 SEM and TEM characterizations

Fig. S2a shows a typical high-magnification SEM image of a sphere with a diameter of about 2.7 µm. It can be observed that the sphere has a highly round and smooth morphology without damage or collapse. A low-magnification TEM image of a sphere with a diameter of 100 nm is presented in Fig. S2b. The corresponding electronic diffraction (ED) pattern in the inset shows a relatively simple crystal structure in this sphere. The major diffraction spots are indexed to be (101) crystal face of rutile. It is found that the crystal structure of a sphere is in relation to its size. The ED patterns of the sub-100 nm spheres mostly exhibit regular discrete spots corresponding to the well-crystallized rutile phase, while that of large-size spheres (>100 nm) are complicated with several spot series, indicating the polycrystalline structure in these spheres.

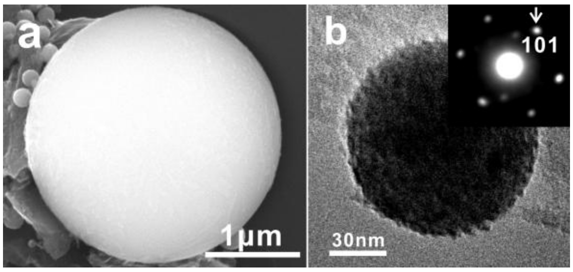

Fig.S2 a) SEM image of a single sphere with a diameter of about 2.7 µm. b) TEM image and the corresponding ED pattern of a small-size sphere with a diameter of 100 nm.

2.3 XPS

Fig.S3 shows the narrow scan Ti XPS spectrum of the spheres. The two peaks at the binding energies of 459.2 eV and 465.1 eV are ascribed to the Ti $2p_{3/2}$ and Ti $2p_{1/2}$ state in TiO_2,[3][4] respectively. It is worth noting that the higher binding energy (465.1 eV) deviates from the standard value (464.9 eV) of TiO_2, which may be due to the distortion of Ti-O bonds, and/or the binding of Ti with N species on the surface part of the sphere.

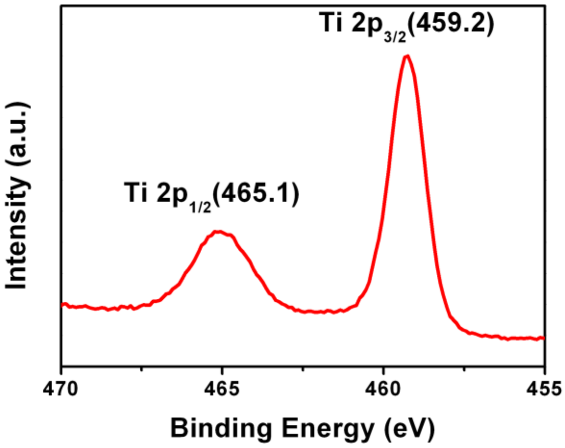

Fig.S3 Narrow scan Ti XPS spectrum of the TiO_2 spheres.

2.4 EDX

Fig. S4 shows the EDX spectrum of the spheres (red line). It should be mentioned that in our experiment, the spheres were deposited on a Si substrate for the EDX characterization, thus the EDX spectrum of the pristine Si substrate without spheres (blue line) is also presented for comparison. It can be concluded from the EDX results that the spheres are mainly composed of Ti and O, which further confirms the TiO_2 composition in the spheres.

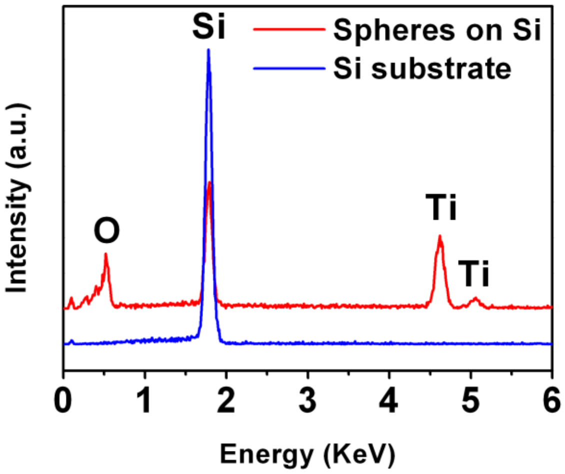

Fig. S4 EDX spectra of the spheres on the Si substrate (red line) and the pristine Si substrate (blue line).

2.5 Calculation results of the density of states and optical adsorption spectra of oxygen-deficient TiO_2

It has been shown that the value of the Hubbard-*U* strongly affects the calculation results.[5] Therefore, in order to obtain an optimal value, several *U* values were considered in our calculations. When *U* is less than 2 eV, the two excess electrons nearly reside at the bottom of the conduction band. Increasing the *U* value further, the defect-related states start to move down into the band gap and form the gap states. For the pristine TiO_2 in the anatase form, a suitable band gap of about 3.1eV can be obtained by employing *U*=4eV, which is in good agreement with the experimental value (~3.2eV). Thus, *U*=4eV was used in all calculations for different oxygen-deficient concentrations.

Figures S5a and S5b show the calculated DOS and the corresponding optical absorption of TiO_{2-x} with x=0, 0.063, 0.125, and 0.25, respectively. The supercells used for the calculations are also presented in the insets of Fig. S5a, and the removed oxygen atom is highlighted with a red dash-line circle. It can be seen that some intermediate states induced by the oxygen vacancies exist between the valence and conduction band, forming the gap states. Following the increase of the oxygen-deficient concentration, the gap states become more extended and their widths are about 0.3eV, 0.5eV and 1.5eV for x=0.063, 0.125 and 0.25, respectively. However, an identical band gap of about 3.1eV is found in each case, including the stoichiometric TiO_2. Similarly, the absorption spectra become stronger and broader when the oxygen-deficient concentration is increased and the absorption spectrum of $TiO_{1.75}$ (25% oxygen-deficient) is closer to the experimental result, as shown in Fig. S5b.

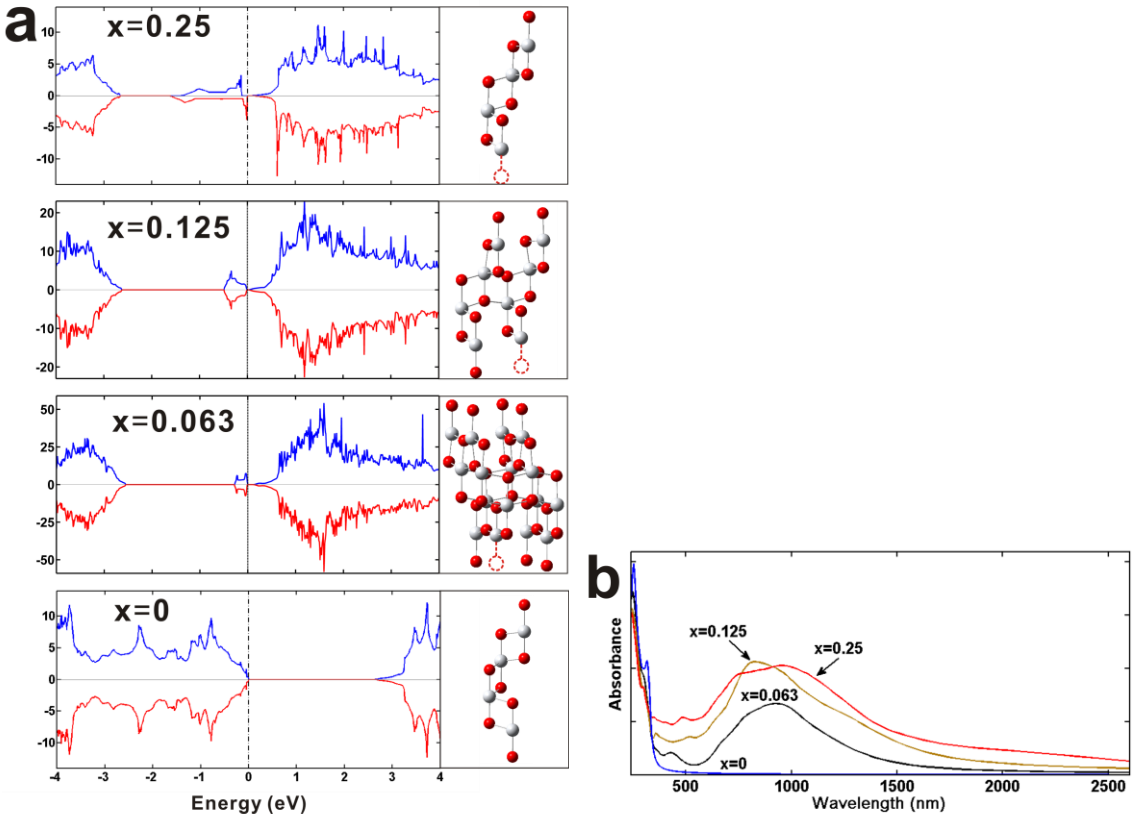

Fig. S5. Density of states (a) and the corresponding optical absorption spectra (b) of oxygen-deficient TiO_{2-x} with x=0, 0.063, 0.125, and 0.25. The insets are the corresponding supercells, in which the removed oxygen atom is highlighted with a red dash-line circle. The dash line denotes the Fermi level. Spin-up and spin-down states are shown above and below the abscissa, respectively.

Supplementary References

[1] K. Azumi, T. Mizuno, T. Akimoto and T. Ohmori, *J. Electrochem. Soc.* 1999, **146**, 3374.

[2] P. W. B. Pearse and A. G. Gaydon, *The Identification of Molecular Spectra*, Chapman & Hall Ltd.: London, **1950**.

[3] M. Murata, K. Wakino and S. Ikeda, *J. Electron Spectrosc. Relat. Phenom.* 1975, **6**, 459.

[4] D. Gonbeau, C. Guimon, G. Pfister-Guillouzo, A. Levasseur, G. Meunier and R. Dormoy, *Surf. Sci.* 1991, **254**, 81.

[5] J. Stausholm-Møller, H. H. Kristoffersen, B. Hinnemann, G. K. H. Madsen and B. Hammer, *J. Chem. Phys.* 2010, **133**, 144708.